

# Bismuth Doping of CdTe: The Effect of Spin–Orbit Coupling

Juan Alberto Ríos-González,\* Eduardo Menéndez-Proupin, and Juan Luis Peña

Using the Heyd, Scuseria, and Ernzerhof (HSE) hybrid functional, with the range-separation parameter modified to match the CdTe bandgap, the electronic structure and thermodynamic properties of bismuth-doped CdTe are calculated. The energy levels associated with bismuth in CdTe bandgap can be obtained only when the spin–orbit coupling (SOC) is included. Substitutional and interstitial Bi atom positions in CdTe lattice are investigated. Contrary to the outcome of calculations without SOC, these simple defects generate bands inside the CdTe bandgap. These bands can act as intermediate steps in two-step light absorption processes that lead to increasing the photocurrent in the solar cell.

## 1. Introduction

Cadmium telluride (CdTe) is a useful semiconductor due to its high absorption coefficient<sup>[1]</sup> and bandgap of 1.49 eV,<sup>[2]</sup> which allows applications for gamma-ray detectors and solar cells.<sup>[3,4]</sup> The CdTe solar cell is the most commercially successful thin-film technology achieving a record 22.1% efficiency.<sup>[5]</sup> Increased efficiency could be achieved by introducing dopants that generate a partially occupied band with energies in the fundamental bandgap. This is called intermediate band (IB). This concept may allow to overcome the theoretical Shockley–Queisser efficiency limit.<sup>[6]</sup> The promotion of electrons from the valence band (VB) to the conduction band (CB) can be enhanced by means of two-step transitions VB→IB→CB energized by sub-bandgap photons, thus increasing the photogenerated current. This concept is known as intermediate band solar cell (IBSC).<sup>[6,7]</sup>

Several doped semiconductors have been proposed as IB materials such as ZnTe:Cr,<sup>[8]</sup> ZnTeO,<sup>[9,10]</sup> V-doped SnS<sub>2</sub>,<sup>[11]</sup> V-substituted In<sub>2</sub>S<sub>3</sub>,<sup>[12]</sup> and GaNAs,<sup>[13]</sup> among others. To obtain the IB, it is necessary to control doping accurately because there is a minimum and maximum doping concentration required to induce the IB. The IB capability to enhance photogeneration is

determined by photogeneration and recombination probabilities. Low doping can cause radiative and nonradiative recombination centers. Recombination can be reduced if in-gap impurity states become delocalized, which requires a relatively high dopant concentration. High doping concentration can lead to agglomerations of doped material, which can compensate the doping effect inducing carrier degradation.<sup>[14–16]</sup>

Furthermore, an experimental study<sup>[17]</sup> has shown an increase in short-circuit current when CdTe solar cells are doped with bismuth. Such increase has been attributed

to an IB. A theoretical study<sup>[18]</sup> also pointed out the presence of an IB in Bi-doped CdTe using the HSE06 screened hybrid functional, associated with several complex defects, such as Bi<sub>i</sub>–V<sub>Cd</sub>, Bi<sub>Cd</sub>–O<sub>Te</sub>, and 2Bi<sub>Cd</sub>. Ríos-González et al.<sup>[19]</sup> have shown that calculations including the spin–orbit coupling (SOC) predict that simple substitutional defects, Bi<sub>Cd</sub>, and Bi<sub>Te</sub>, can also generate an IB. In this work, the role of interstitial Bi has been included and compared with substitutional Bi. The obtained electronic structure supports the hypothesis that Bi can generate an IB in CdTe.

## 2. Methodology

### 2.1. Electronic Structure Calculations

Density functional theory (DFT) has been used to calculate the energy bands of Bi-doped CdTe. The plane-wave projector augmented wave (PAW) scheme has been used,<sup>[20,21]</sup> as implemented in the Vienna Ab Initio Simulation Package (VASP).<sup>[22]</sup> The exchange and correlation effects have been included using the hybrid functional proposed by Heyd, Scuseria, and Ernzerhof (HSE).<sup>[23]</sup> When SOC is included in calculations with the HSE functional, a bandgap of 1.2 eV is obtained for CdTe. To match the CdTe experimental bandgap of 1.5 eV, the range-separation parameter  $\omega$  in the HSE functional has been modified to  $\omega = 0.0811 \text{ \AA}^{-1}$ , referring to this functional as HSE( $\omega$ ) + SOC (see Appendix 1). It is known that defect states and host states may need different screening parameters, and fake in-gap states may appear due to supercell size effect with hybrid functionals.<sup>[24,25]</sup> Hence, it was verified that with our setup, the perfect CdTe supercell with either an extra hole or an extra electron (charge 1+ and 1–) does not show in-gap states. The wavefunctions have been expanded in plane waves with cutoff energy of 265 eV, obtaining converged forces and total energies with the library of PAW potentials for many-body GW calculation. To verify that the structural properties and the total energies of

Dr. J. A. Ríos-González, Dr. J. L. Peña

Departamento de Física Aplicada

CINVESTAV Unidad Mérida

97310 Mérida, México

E-mail: juan.rios@cinvestav.mx


Prof. E. Menéndez-Proupin

Departamento de Física

Facultad de Ciencias

Universidad de Chile

Las Palmeras 3425, 780-0003 Ñuñoa, Santiago, Chile

 The ORCID identification number(s) for the author(s) of this article can be found under <https://doi.org/10.1002/pssb.201900693>.

DOI: 10.1002/pssb.201900693

CdTe are well described, the lattice parameter and bulk modulus were obtained by fitting the Birch–Murnaghan equation of state. The obtained values of 6.54 Å and 41.05 GPa are close to experimental values of 6.481 and 44.5 GPa, respectively.<sup>[26]</sup>

In our model, the Bi impurity was placed at Cd or Te positions or at interstitial sites in a CdTe 64-atom supercell (SC64). The system was sampled in the reciprocal space with  $\Gamma$ -centered  $2 \times 2 \times 2$   $k$ -point grid. Each impurity model was relaxed using the general-gradient approximation (GGA) exchange-correlation functional as proposed by Perdew, Burke, and Ernzerhof (PBE).<sup>[27]</sup> Afterward, the relaxation was refined using the HSE( $\omega$ ) functional without SOC, and finally, one last relaxation was conducted with HSE( $\omega$ ) + SOC. The relaxed structures are provided in the Supporting Information. The CdTe heat of formation  $\Delta H(\text{CdTe})$  calculated with PBE was  $-0.78$  eV, whereas HSE( $\omega$ ) + SOC gave a value of  $-1.19$  eV. The latter value is close to the experimental one of  $-1.04$  eV.<sup>[28]</sup> The energy of bulk Cd has been found relaxing the 2-atom crystallographic unit cell, sampling the Brillouin zone with a  $22 \times 22 \times 22$   $k$ -point grid. Similarly, the energy of bulk Te has been obtained relaxing the crystallographic 3-atom unit cell with the Brillouin zone sampled with a  $9 \times 9 \times 9$   $k$ -point grid. The energy of bulk Bi has been computed with an  $8 \times 8 \times 8$   $k$ -points grid in the Brillouin zone using a 6-atom unit cell.

The formation energy of substitutional and interstitial bismuth impurities,  $\text{Bi}_x$  ( $x = \text{Cd}, \text{Te}, \text{ic}$  [interstitial surrounded by cations] or  $\text{ia}$  [interstitial surrounded by anions]), has been calculated as the difference between the global energy of a SC64, and the energy of the same supercell with the impurity. The chemical potentials of Bi, and the released Cd or Te (in substitutional case) must be included in the formation energy. For example, the formation energy of  $\text{Bi}_{\text{Cd}}$  is

$$\begin{aligned} \Delta H_f(\text{Bi}_{\text{Cd}}^q) = & E(\text{BiCd}_{n-1}\text{Te}_n) + [E(\text{Cd}) + \Delta\mu_{\text{Cd}}] \\ & - E(\text{Cd}_n\text{Te}_n) - [E(\text{Bi}) + \Delta\mu_{\text{Bi}}] \\ & + q[E_V + E_F] + \Delta E_{\text{size}} \end{aligned} \quad (1)$$

where  $n = 32$  for the SC64 model. To obtain the formation energy of interstitial Bi, it is enough to drop the term  $[E(\text{Cd}) + \Delta\mu_{\text{Cd}}]$  in Equation (1) and change  $n - 1$  by  $n$ . The formation energy of  $\text{Bi}_{\text{Te}}$  is obtained by the exchange of Cd with Te in Equation (1). The term  $E(\text{Cd})$  is the energy of bulk Cd, computed, as described earlier.  $\Delta\mu_{\text{Cd}}$  is the chemical potential relative to the reference state, which depends on the thermodynamic equilibrium conditions. In Cd-rich condition  $\Delta\mu_{\text{Cd}} = 0$ , whereas in Cd-poor conditions (or Te-rich conditions)  $\Delta\mu_{\text{Cd}}$  has the value of the heat of formation  $\Delta H(\text{CdTe})$ .<sup>[29]</sup> For a charged defect,  $q$  is the number of electrons donated to the environment.  $E_V + E_F$  is the electron chemical potential, where  $E_F$  is the Fermi level relative to the VB maximum  $E_V$ . For dilute impurities, it is necessary to include size corrections (included in Appendix 2),  $\Delta E_{\text{size}}$ , that are described in a previous study.<sup>[30]</sup> Appendix 2 shows that the size-corrected formation energies computed at PBE level with SC64s closely approximate the results obtained with 512-atom supercells. Thermodynamic conditions to prevent precipitation of Bi or  $\text{Bi}_2\text{Te}_3$  are included by means of the following restrictions on chemical potentials:

$$\Delta\mu_{\text{Bi}} \leq 0 \quad (2)$$

$$2\Delta\mu_{\text{Bi}} + 3\Delta\mu_{\text{Te}} \leq \Delta H(\text{Bi}_2\text{Te}_3) \quad (3)$$

Here, the calculated  $\text{Bi}_2\text{Te}_3$  heat of formation has a value of  $\Delta H(\text{Bi}_2\text{Te}_3) = -0.90$  eV. The expressions in Equation (2) and (3) implies that in Te-rich condition,  $\Delta\mu_{\text{Bi}} \leq -0.45$  eV, whereas in Cd-rich conditions,  $\Delta\mu_{\text{Bi}} \leq 0$ . The equalities have been considered for the results shown in Section 2.3, understanding that the reported formation energies are minimum values.

## 2.2. Electronic Structure

This section corresponds to the analysis of the band structure of different defects,  $\text{Bi}_{\text{Cd}}$ ,  $\text{Bi}_{\text{Te}}$ ,  $\text{Bi}_{\text{ic}}$ , and  $\text{Bi}_{\text{ia}}$ , which is shown in Figure 1, along with the projected density of states (PDOS). The band diagrams and density of states (DOS) have been calculated for SC64 models with the HSE( $\omega$ ) + SOC formalism.

### 2.2.1. $\text{Bi}_{\text{Cd}}$

The  $\text{Bi}_{\text{Cd}}$  impurity assumes a configuration with  $T_d$  symmetry, where the bonds Te–Bi have a length of 3.09 Å (Figure 2b). A defect complex  $V_{\text{Cd}} + \text{Bi}_i$  results in the relaxation of Bi atom into the position of the vacancy of cadmium. Figure 1b shows the band structure calculated for  $\text{Bi}_{\text{Cd}}$  defect. The impurity creates a flat band below the conduction band minimum (CBM). This in-gap band is nondegenerate, and it is occupied in the neutral state. In the  $\Gamma$  point, the IB is 0.23 eV below the CBM. The charge state 1+ is also possible, therefore, the defect  $\text{Bi}_{\text{Cd}}$  is a donor. To take advantage of the IB solar cell, it is necessary to obtain a half-filled IB.<sup>[6]</sup> This can be achieved in combination with acceptor impurities or intrinsic defects, e.g.,  $V_{\text{Cd}}$ .

### 2.2.2. $\text{Bi}_{\text{Te}}$

The band structure of  $\text{Bi}_{\text{Te}}$  in the SC64 model is shown in Figure 1c. This defect is a deep acceptor with charge states 0 and 1–, and it can create a nondegenerate IB. The IB energy at the  $\Gamma$  point is 0.80 eV below the CBM. The PDOS shows that the contribution to the IB comes from Bi and Te atoms. These are the second neighbors of Bi as the first neighbors are Cd atoms. The top of the VB is also modified by the impurity. The Te 5p orbitals give the largest contribution to the upper part of the VB in pure CdTe.<sup>[31]</sup> The presence of the impurity splits the valence band maximum (VBM) and originates a complex band structure with dispersion, due to Bi and Te orbitals. This effect is expected to disappear for a lower Bi concentration, which can be modeled with a larger supercell.<sup>[30]</sup>

### 2.2.3. $\text{Bi}_{\text{ic}}$

As shown in Figure 1d, bismuth in a cation interstitial site generates a double band inside the CdTe bandgap. According to the PDOS, both bands arise from bismuth interaction with tellurium second neighbors (recall that the bismuth is surrounded by cadmium atoms). These bands are 0.66 and 0.89 eV above the VBM, and they are completely occupied in the neutral

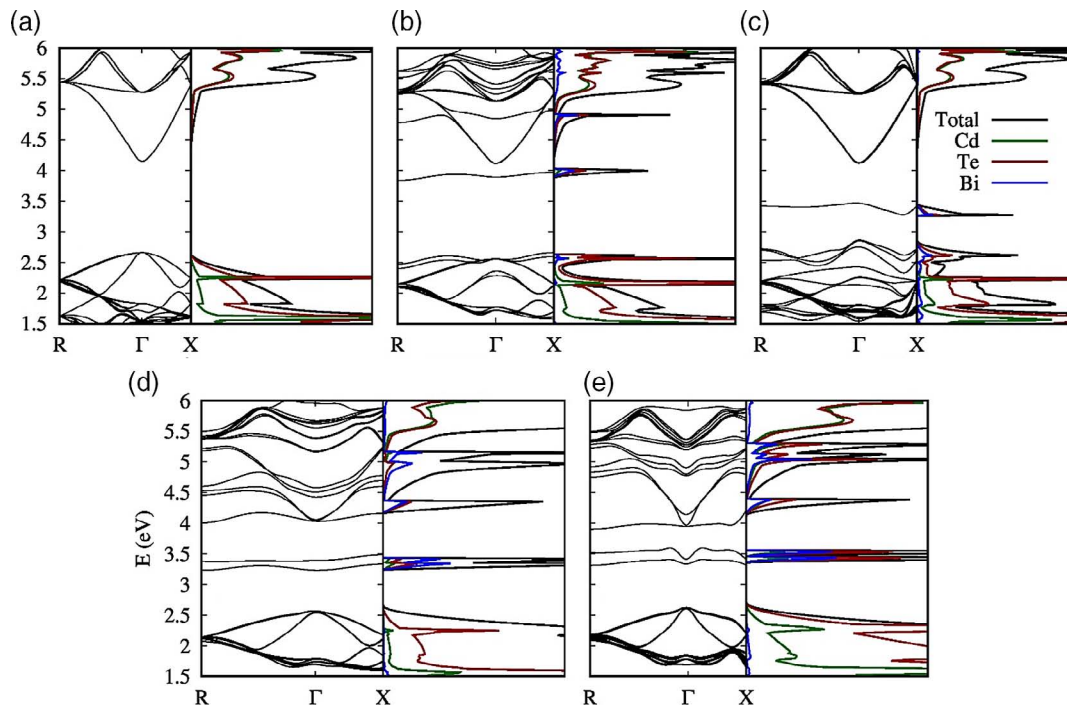


**Figure 1.** Band structures and PDOSs of a) CdTe, and the defects b)  $\text{Bi}_{\text{Cd}}$ , c)  $\text{Bi}_{\text{Te}}$ , d)  $\text{Bi}_{\text{iC}}$ , and e)  $\text{Bi}_{\text{iA}}$ , performed with a SC64. All band structures for the defective SC64 were calculated in neutral charge state.

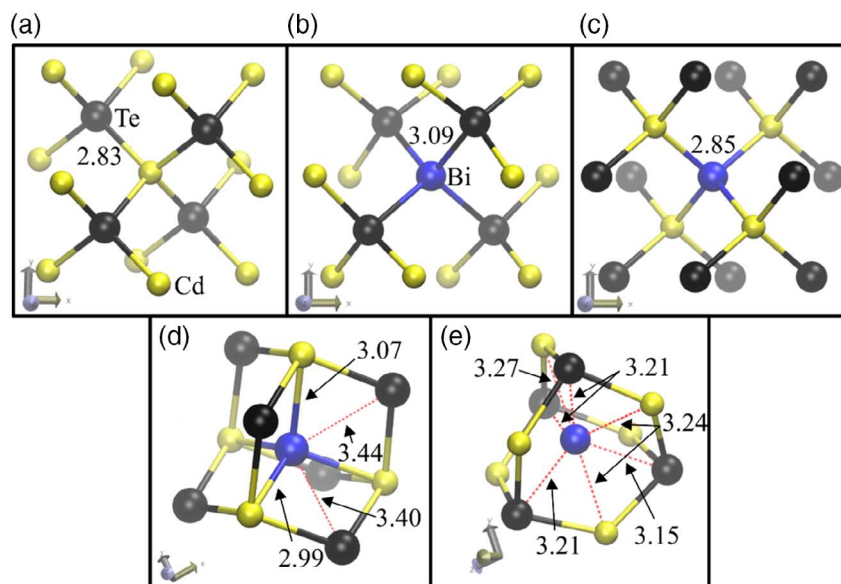


**Figure 2.** The structural model shows the atomic distance in each case after relaxation with HSE( $\omega$ ) + SOC. Black, yellow, and blue balls represent Te, Cd, and Bi atoms, respectively. a) Perfect CdTe, b)  $\text{Bi}_{\text{Cd}}$ , c)  $\text{Bi}_{\text{Te}}$ , d)  $\text{Bi}_{\text{iC}}$ , and e)  $\text{Bi}_{\text{iA}}$ .

state. The Bi—Cd bond distances are 2.99 and 3.07 Å (Figure 2d), respectively. This defect is stable; however, near a cadmium vacancy, it is unstable. In our calculations, the complex defect  $V_{\text{Cd}} + \text{Bi}_{\text{i}}$  relaxes to a  $\text{Bi}_{\text{Cd}}$  defect. Although the size of the Bi atom may prevent its diffusion across the lattice, diffusion of Cd vacancies may lead to annihilation of this defect.

#### 2.2.4. $\text{Bi}_{\text{iA}}$

As shown in Figure 2e, the distance between Bi and its first neighbor (Te) is greater than for  $\text{Bi}_{\text{iC}}$ . This causes a considerable distortion in the CdTe lattice. As shown in Figure 1e, two bands appear near the bandgap center, as well as another flat band that

is degenerate with the CBM at the  $\Gamma$  point. The bands inside the bandgap are totally occupied. Therefore, this is a deep donor. The PDOS shows the main Bi character of these bands.

### 2.3. Formation Energy of Isolated Defects

Using the SC64 model, the formation energies have been calculated (Figure 3). For  $\text{Bi}_{\text{Cd}}$ , the stable charge states for Fermi level inside of the CdTe bandgap are neutral and 1+, with the transition level  $\epsilon(1+/0) = 1.30$  eV. The stable charge states for  $\text{Bi}_{\text{Te}}$  are 1+, 0, and 1-. The transition levels are  $\epsilon(1+/0) = 0.25$  and  $\epsilon(0/1-) = 0.64$  eV. For  $\text{Bi}_{\text{ic}}$ , the stable charge states are 2+ and 1+. The transition level for this defect is  $\epsilon(2+/1+) = 0.45$  eV. Finally, the defect  $\text{Bi}_{\text{ia}}$  is stable in 3+, 2+, and 1+ charge states with transition levels  $\epsilon(3+/2+) = 0.32$  and  $\epsilon(2+/1+) = 0.66$  eV.

The Cd- or Te-richness modifies the relative stability of the defects as described by the chemical potential terms in Equation (1). Figure 3 shows that in Cd-rich condition  $\text{Bi}_{\text{Te}}$  has the lower formation energy, it means that this is the most plausible defect in thermodynamic equilibrium. In contrast, for Te-rich condition,  $\text{Bi}_{\text{Cd}}$  is the most plausible defect. For this reason, by controlling the Cd- and Te-rich conditions the defect can be changed.

The computed formation energies constitute rough estimations for the limit of isolated defects. The bismuth concentration in SC64s is higher than the nominal concentrations reported in experimental works.<sup>[17,32]</sup> Regrettably, the high cost of the calculation with SOC and hybrid functional has not allowed us to use larger supercells. The size-effect corrections mitigate the error, but one cannot discard the effect of excessive Bi concentration on the quantum state obtained, as has been shown for the tellurium vacancy.<sup>[30]</sup> In any case, the calculation in this work makes clear that substitutional Bi is energetically favored over interstitial Bi. The relatively high values of  $\text{Bi}_{\text{ic}}$  and  $\text{Bi}_{\text{ia}}$  energies indicate the low stability against the substitutional defects, as well as high barriers for Bi diffusion.

For an IB absorber material, it is necessary to achieve high dopant concentration, and the whole material must be neutral. Therefore, the impurities must be neutral or must be compensated by another highly concentrated impurity. The formation

energies of neutral  $\text{Bi}_{\text{Te}}$  and  $\text{Bi}_{\text{Cd}}$  are rather high, hence the material is not thermodynamically stable. However, the large size of Bi implies that it should have low diffusion coefficient, allowing the material to be stable kinetically. It remains to be determined what is the real concentration of bismuth, in opposition to the reported nominal concentration.<sup>[17,32]</sup>

The implantation of bismuth can be favored in a charge state of low formation energy. This could be attained using a co-dopant with the opposite charge. For example, substitutional chlorine ( $\text{Cl}_{\text{Te}}$ ) is a well-known donor<sup>[33,34]</sup> that favors the presence of compensating acceptors like  $\text{V}_{\text{Cd}}$ , or  $\text{Bi}_{\text{Te}}$ . The extended practice of  $\text{CdCl}_2$  treatment may explain the successful reports of Bi implantation in CdTe.<sup>[17,32]</sup> Alternatively,  $\text{Bi}_{\text{Cd}}$  could be favored by codoping with an acceptor group I<sup>[35,36]</sup> or group V element.<sup>[37–40]</sup> Diffusion of these species out of the material<sup>[36]</sup> would let  $\text{Bi}_{\text{Te}}$  in neutral charge state.

Let us stress that the role of IBs is not to modify the n- or p-type character, but to increase the carriers in the VB and CB taking advantage of sub-bandgap photons. The IB material must be confined within regions lacking IB, and the charge carriers must be able to reach these regions before recombination. While the latest issue cannot be assessed from our research, the issue of confining the IB region seems feasible because the large size of the Bi atoms should hinder its diffusion.

Another interesting issue is the delocalization of the Bi-induced deep levels. Localization arises for low impurity concentration induced by disorder (Anderson transition) by electronic correlation (Mott transition). The minimal concentration to have delocalized states cannot be directly obtained from our periodic DFT calculations, which provide delocalized band states by construction for any impurity concentration. Hence, the bands presented in this report are meaningful, and useful for IBSC, if the Bi concentration is higher than the, still unknown, threshold concentration. Furthermore, the IB states may not necessarily grant efficient optical transitions. These questions merit further investigation. To the best of our knowledge, the results obtained in the study by Vigil-Galán et al.<sup>[17]</sup> are the sole experimental evidence of the IB effect in Bi-doped CdTe.

### 3. Conclusions

To obtain accurate band structures of CdTe doped with Bi, an adapted HSE hybrid functional has been used. The HSE range-separation parameter was adjusted to the value  $\omega = 0.0811 \text{ \AA}^{-1}$ , which allows to reproduce the CdTe experimental bandgap. This adjusted functional was used to study different simple defects such as bismuth impurities in interstitial and substitutional positions to show active levels inside the CdTe bandgap. The results indicate that the presence of Bi in different positions in the CdTe lattice can cause deep levels in its bandgap. Interstitial Bi is less stable than substitutional Bi in the CdTe lattice, as confirmed by energy calculations. According to the formation energy, the thermodynamically more stable defects are  $\text{Bi}_{\text{Te}}$  and  $\text{Bi}_{\text{Cd}}$  for Cd-rich and Te-rich conditions, respectively. Usually, CdTe is deposited with close space sublimation technique, allowing Cd-rich conditions.<sup>[41,42]</sup> For this reason, the most important defect is  $\text{Bi}_{\text{Te}}$ , which can induce an IB at 0.8 eV below to the CBM. The in-gap position of the

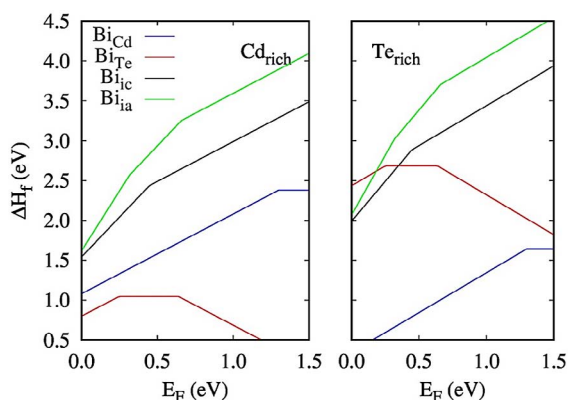


**Figure 3.** Formation energies of  $\text{Bi}_{\text{Cd}}$ ,  $\text{Bi}_{\text{Te}}$ ,  $\text{Bi}_{\text{ic}}$ , and  $\text{Bi}_{\text{ia}}$ , as a function of the Fermi level.

IB is achieved only when the SOC is included in the calculations. The results using the hybrid functional HSE( $\omega$ ) without SOC do not show the contribution in the levels inside of CdTe bandgap for the simple defects considered. Bi<sub>Te</sub> also causes the least distortion in the CdTe lattice. The increase in the short-circuit current presented in the study by Vigil-Galán et al.<sup>[17]</sup> for Bi-doped CdTe solar cells could be explained with our results.

## Appendix 1

### Validation of the HSE( $\omega$ ) Functional

By means of comparison with GW calculations, the accuracy of the functional in predicting the VB and CB edges can be assessed. **Figure A1** shows the bandgap, the CBM, and the VBM, computed using the functional HSE( $\omega$ ) + SOC for different values of the range separation parameter  $\omega$ , as well as with the PBE0 method and the  $G_0W_0$  approximation. The  $G_0W_0$  calculation was carried out starting from wavefunctions computed with the HSE06 functional, including SOC, for the 2-atom primitive cell. The number of bands was studied up to 1600 (18 occupied), but 800 were found enough to obtain the quasi-particle energies within 0.01 eV. An  $8 \times 8 \times 8$  k-point grid, a 169.4 eV cutoff for the response function, and 96 frequencies were used. The obtained bandgap was 1.56 eV, which is very close to the experimental bandgap at low temperature.<sup>[43]</sup>

The HSE functional has two parameters, the fraction of exact exchange  $\alpha$ , and the range-separation parameter  $\omega$ . In the standard HSE06,  $\alpha = 0.25$  and  $\omega = 0.2 \text{ \AA}^{-1}$ , the latter being the result of fitting for a group of semiconductors.<sup>[27]</sup> In contrast, for  $\omega = 0$  one obtains the PBE0 functional, which in its standard form has  $\alpha = 0.25$ . As shown in Figure A1, PBE0 (with  $\alpha = 0.25$ ) gives a too large bandgap of 1.86 eV. All calculations are including SOC. In contrast, HSE06 gives a too small bandgap of 1.2 eV. It is widely practiced adjusting the parameter of exact exchange  $\alpha$  in HSE, or PBE0 to fit the bandgap. For PBE0, it has been argued that  $\alpha$  must be equal to the inverse of the high-frequency dielectric constant  $1/\epsilon_\infty$ .<sup>[44]</sup> However, this leads to a too small bandgap in CdTe. PBE0 with  $\alpha = 0.20$  fits the bandgap,

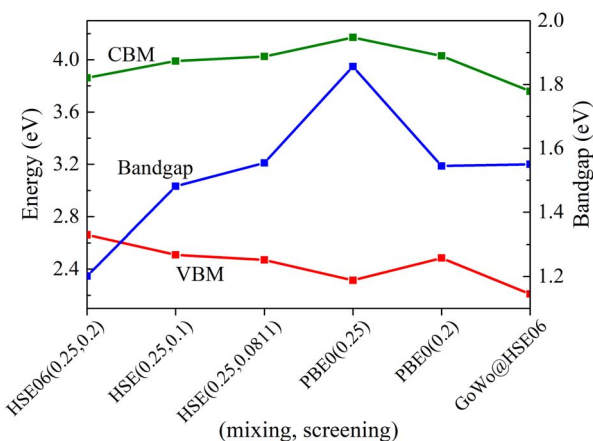


**Figure A1.** Bandgap, VB maximum, and CB minimum of CdTe, with different parameters of the HSE and PBE0 functionals, compared with  $G_0W_0$ .

as well as HSE with  $\alpha = 0.25$  and  $\omega = 0.0811 \text{ \AA}^{-1}$ . The latter, HSE(0.25, 0.0811), can be regarded as an interpolation between HSE06 and PBE0. The energies of the VBM and CBM are 0.26 eV above the  $G_0W_0$  values. Regarding the band edges, the  $G_0W_0$  VBM energy is best approximated by the PBE0 functional, whereas the CBM is best approximated by the HSE06 functional. The bandgap is best approximated by HSE(0.25, 0.0811) and PBE0(0.20).

## Appendix 2

### Size Corrections

**Table A1** shows the different size corrections applied to obtain the formation energies in the dilute limit. The size correction is obtained as the sum

$$\Delta E_{\text{size}} = \Delta E_{\text{b.f.}} + \Delta E_{\text{p.a.}} + \Delta E_{\text{L-Z}}. \quad (\text{A1})$$

All the terms have been calculated as described in the study by Menéndez-Proupin and Orellana.<sup>[30]</sup> The first term is the band-filling correction, applied for charge states that contain electrons in the CB or holes in the VB. The second term is the potential alignment correction, needed to align the energy scales of the defect supercells and the pristine CdTe. This correction is applied to the energies of non-neutral supercells. The last term

**Table A1.** Size corrections to the formation energies (in eV) using the HSE + SOC functional for SC64. The blank spaces correspond to values not required in the energy formation calculation.

Correction	Charge state				
	1-	0	1+	2+	3+
Defect: Bi <sub>Cd</sub>					
$\Delta E_{\text{b.f.}}$		0	0		
$\Delta E_{\text{p.a.}}$		0	0.14		
$\Delta E_{\text{L-Z}}$		0	0.08		
$\Delta E_{\text{size}}$		0	0.22		
Defect: Bi <sub>Te</sub>					
$\Delta E_{\text{b.f.}}$	0	0	0		
$\Delta E_{\text{p.a.}}$	0.09	0	0.04		
$\Delta E_{\text{L-Z}}$	0.08	0	0.08		
$\Delta E_{\text{size}}$	0.17		0.12		
Defect: Bi <sub>ic</sub>					
$\Delta E_{\text{b.f.}}$			0	0	0
$\Delta E_{\text{p.a.}}$			0.07	0.52	1.02
$\Delta E_{\text{L-Z}}$			0.08	0.34	0.76
$\Delta E_{\text{size}}$			0.15	0.86	1.78
Defect: Bi <sub>ia</sub>					
$\Delta E_{\text{b.f.}}$			0	0	
$\Delta E_{\text{p.a.}}$			0.22	0.55	0.93
$\Delta E_{\text{L-Z}}$			0.08	0.34	0.76
$\Delta E_{\text{size}}$			0.30	0.89	1.66

corrects the interaction of the charges localized at the defects with its periodic images, following the scheme proposed by Lany and Zunger.<sup>[45]</sup> To assess the accuracy of this size corrections, the formation energies have been computed with the efficient PBE functional with a 512-atom supercell, and they have been compared with the results from the SC64 in the same approximation.

Recalling Equation (1), we can define the difference between the formation energies computed with both supercell models, as

$$\Delta H_f(512) - \Delta H_f(64) = E(\text{Cd}_{256}\text{Te}_{256} + X) - E(\text{Cd}_{256}\text{Te}_{256}) - [E(\text{Cd}_{64}\text{Te}_{64} + X) - E(\text{Cd}_{64}\text{Te}_{64})] \quad (\text{A2})$$

Or, including the size effect corrections

$$\Delta H_f(512) - \Delta H_f(64) = E(\text{Cd}_{256}\text{Te}_{256} + X) - E(\text{Cd}_{256}\text{Te}_{256}) - [E(\text{Cd}_{32}\text{Te}_{32} + X) - E(\text{Cd}_{32}\text{Te}_{32})] + \Delta E_{\text{size}}(512) - \Delta E_{\text{size}}(64) \quad (\text{A3})$$

For 512-atom supercell, only the  $\Gamma$  point is used, therefore  $\Delta E_{\text{b.f}}(512) = 0$ .  $\Delta E_{\text{L-Z}}(512)$  is half  $\Delta E_{\text{L-Z}}(64)$ .

**Table A2.** Size corrections to the formation energies (in eV) using the PBE functional for both SC64s and 512-atom supercells. The blank spaces correspond to values not required in the energy formation calculation. In the size corrections ( $\Delta E$ ), the values correspond to 64-atom/512-atom supercell. In the  $\Delta H_f$  box, the upper value corresponds to the difference without size corrections and the one below corresponds to the difference including the size correction.

Correction	Charge state				
	1-	0	1+	2+	3+
Defect: Bi <sub>Cd</sub>					
$\Delta E_{\text{b.f.}}$		-0.614/0	0/0		
$\Delta E_{\text{p.a.}}$		0/0	0.134/0.051		
$\Delta E_{\text{L-Z}}$		0/0	0.085/0.042		
$\Delta E_{\text{size}}$		-0.614/0	0.219/0.093		
$\Delta H_f(512)$		-0.638	0.059		
$-\Delta H_f(64)$		-0.024	-0.067		
Defect: Bi <sub>Te</sub>					
$\Delta E_{\text{b.f.}}$	0/0	-0.031/0	-0.097/0		
$\Delta E_{\text{p.a.}}$	0.076/0.037	0/0	-0.053/0.006		
$\Delta E_{\text{L-Z}}$	0.085/0.042	0/0	0.085/0.042		
$\Delta E_{\text{size}}$	0.161/0.079	-0.031/0	-0.065/0.048		
$\Delta H_f(512)$	0.070	0.058	0.045		
$-\Delta H_f(64)$	0.012	0.089	0.158		
Defect: Bi <sub>ia</sub>					
$\Delta E_{\text{b.f.}}$		0/0			0/0
$\Delta E_{\text{p.a.}}$		0/0			0.855/0.396
$\Delta E_{\text{L-Z}}$		0/0			0.765/0.382
$\Delta E_{\text{size}}$		0/0			1.620/0.778
$\Delta H_f(512)$		-0.215			0.875
$-\Delta H_f(64)$		-0.215			0.033

It is known<sup>[30]</sup> that different functionals can lead to different atomic arrangements around defects. Hence, the PBE formation energies  $\Delta H_f(64)$  have been computed with the atomic positions obtained with HSE( $\omega$ ) + SOC, without further relaxation. To obtain  $\Delta H_f(512)$ , Bi-centered clusters were built from the SC64s and were embedded in perfect 512-atom supercells. The atomic positions of the atoms that remain out of the clusters were relaxed. The size corrections with both 64- and 512-atom models are shown in Table A2. Comparing values of Table A1 and A2 for the 64-atom model, one can appreciate significant differences that are due to the change of functional. For example, the band-filling corrections for Bi<sub>Cd</sub> in neutral charge state are completely different with HSE( $\omega$ ) + SOC and PBE. This happens because with PBE, there is no IB like with HSE( $\omega$ ) + SOC, and the highest occupied level is the CB. For this state, the size correction in the 64-atom model is -0.614 eV, whereas for 512-atom model there is no correction. The difference of formation energies is -0.638 eV when evaluated by Equation A(1), but when the size effect correction is included with Equation A(2), the difference reduces to -0.024. For the other impurities and charge states, the difference is also small. The biggest difference is for Bi<sub>ia</sub>(0), for which no size correction is applicable. At PBE level, Bi<sub>ia</sub>(0) has the CB resonant with the defect bands, resulting in three electrons occupying four bands. No band filling correction was applied, as done with the hybrid functional. If the band filling correction is applied to these bands, -1.28 eV is obtained. If only the top three bands are considered, containing one electron, a correction of -0.50 eV is found. In this case, the explicit calculation with a large supercell is the only safe approach. However, the difference of -0.215 eV is reasonably small. Therefore, we believe that the formation energies obtained at HSE( $\omega$ ) + SOC with the small SC64s are meaningful.

## Supporting Information

Supporting Information is available from the Wiley Online Library or from the author.

## Acknowledgements

This work was supported by the CONICYT FONDECYT regular grants No. 1130437, and 1171807, CONACYT-SENER SUSTENTABILIDAD ENERGÉTICA (México) under project CeMIE-Sol PY-207450/P25 and Consolidación del Laboratorio de Energía Renovable del Sureste (LENERSE) 254667. J.A.R.-G. thanks CONACYT fellowships (for PhD@México 485215 and visit to Chile). Powered@NLHPC: This research was partially supported by the supercomputing infrastructure of the NLHPC (ECM-02). ABACUS at CINVESTAV-IPN is acknowledged for allocations of computational resources under the project CONACYT-EDOMEX-2011-C01-165873. P. Wahnón and coworkers at Universidad Politécnica de Madrid are acknowledged for introductory discussions.

## Conflict of Interest

The authors declare no conflict of interest.

## Keywords

density functional theory, doping, intermediate bands, solar cells, spin-orbit coupling

Received: November 4, 2019

Revised: May 12, 2020

Published online:

- 
- [1] A. E. Rakhshani, *J. Appl. Phys.* **1997**, *81*, 7988.  
 [2] M. Powalla, S. Paetel, E. Ahlswede, R. Wuerz, C. D. Wessendorf, T. M. Friedlmeier, *Appl. Phys. Rev.* **2018**, *5*, 041602.  
 [3] R. E. Kremer, W. B. Leigh, *J. Cryst. Growth* **1988**, *86*, 490.  
 [4] A. Rios-Flores, O. Arés, J. M. Camacho, V. Rejón, J. L. Peña, *Sol. Energy* **2012**, *86*, 780.  
 [5] First Solar Inc., First Solar Press Release, **2016**, <https://investor.firstsolar.com/news/press-release-details/2016/First-Solar-Achieves-Yet-Another-Cell-Conversion-Efficiency-World-Record/default.aspx>, (accessed: October 2019).  
 [6] A. Luque, A. Martí, *Phys. Rev. Lett.* **1997**, *78*, 5014.  
 [7] A. Luque, A. Martí, C. Stanley, *Nat. Photonics* **2012**, *6*, 146.  
 [8] K. S. Lee, G. Oh, E. K. Kim, *Sol. Energy* **2018**, *164*, 262.  
 [9] T. Tanaka, K. M. Yu, Y. Okano, S. Tsutsumi, S. Haraguchi, K. Saito, Q. Guo, M. Nishio, W. Walukiewicz, *IEEE J. Photovolt.* **2017**, *7*, 1024.  
 [10] W. Wang, A. S. Lin, J. D. Phillips, *Appl. Phys. Lett.* **2009**, *95*, 011103.  
 [11] Y. Seminovski, P. Palacios, P. Wahnón, *J. Phys.: Condens. Matter* **2014**, *26*, 395501.  
 [12] R. Lucena, J. C. Conesa, I. Aguilera, P. Palacios, P. Wahnón, *J. Mater. Chem. A* **2014**, *2*, 8236.  
 [13] N. López, L. A. Reichertz, K. M. Yu, K. Campman, W. Walukiewicz, *Phys. Rev. Lett.* **2011**, *106*, 028701.  
 [14] D. J. Chadi, *Phys. Rev. B* **1999**, *59*, 15181.  
 [15] J. J. Krich, B. I. Halperin, A. Aspuru-Guzik, *J. Appl. Phys.* **2012**, *112*, 013707.  
 [16] A. Luque, A. Martí, E. Antolín, C. Tablero, *Physica B: Condens. Matter* **2006**, *382*, 320.  
 [17] O. Vigil-Galán, M. Courel, F. Cruz-Gandarilla, D. Seuret-Jiménez, *J. Mater. Sci: Mater. Electron* **2016**, *27*, 6088.  
 [18] Y. Seminovski, P. Palacios, P. Wahnón, *Sol. Energy Mater. Sol Cells* **2013**, *114*, 99.  
 [19] J. A. Ríos-González, E. Menéndez-Proupin, J. L. Peña, *J. Phys. Conf. Ser.* **2018**, *1043*, 012044.  
 [20] P. E. Blöch, *Phys. Rev. B* **1994**, *50*, 17953.  
 [21] G. Kresse, D. Joubert, *Phys. Rev. B* **1999**, *59*, 1758.  
 [22] G. Kresse, J. Furthmüller, *Phys. Rev. B* **1996**, *54*, 11169.  
 [23] J. Heyd, G. E. Scuseria, M. Ernzerhof, *J. Chem. Phys.* **2006**, *124*, 219906.  
 [24] S. Lany, A. Zunger, *Phys. Rev. B* **2010**, *81*, 205209.  
 [25] J. Bang, Y. Y. Sun, T. A. Abtew, A. Samanta, P. Zhang, S. B. Zhang, *Phys. Rev. B* **2013**, *88*, 035134.  
 [26] B. K. Agrawal, S. Agrawal, *Phys. Rev. B* **1992**, *45*, 8321.  
 [27] J. P. Perdew, K. Burke, M. Ernzerhof, *Phys. Rev. Lett.* **1996**, *77*, 3865.  
 [28] R. F. Brebrick, *J. Phase Equilib. Diffus.* **2010**, *31*, 260.  
 [29] S-H. Wei, S. B. Zhang, *Phys. Rev. B* **2002**, *66*, 155211.  
 [30] E. Menéndez-Proupin, W. Orellana, *Phys. Status Solidi B* **2015**, *252*, 2649.  
 [31] E. Menéndez-Proupin, G. Gutiérrez, E. Palmero, J. L. Peña, *Phys. Rev. B* **2004**, *70*, 035112.  
 [32] C. M. Ruiz, O. Vigil, E. Saucedo, G. Contreras-Puente, V. Bermúdez, *J. Phys.: Condens. Matter* **2006**, *18*, 7163.  
 [33] J-H. Yang, W-J. Yin, J-S. Park, W. Metzger, S-H. Wei, *J. Appl. Phys.* **2016**, *119*, 045104.  
 [34] W. Orellana, E. Menéndez-Proupin, M. A. Flores, *Sci. Rep.* **2019**, *9*, 9194.  
 [35] J. Ma, S-H. Wei, T. A. Gessert, K. K. Chin, *Phys. Rev. B* **2011**, *83*, 245207.  
 [36] H-X. Deng, J-W. Luo, S-S. Li, S-H. Wei, *Phys. Rev. Lett.* **2016**, *117*, 165901.  
 [37] J. M. Burst, J. N. Duenow, D. S. Albin, E. Colegrove, M. O. Reese, J. A. Aguilar, C-S. Jiang, M. K. Patel, M. M. Al-Jassim, D. Kuciauskas, S. Swain, T. Ablekim, K. G. Lynn, W. K. Metzger, *Nat. Energy* **2016**, *1*, 16015.  
 [38] M. A. Flores, W. Orellana, E. Menéndez-Proupin, *Phys. Rev. B* **2017**, *96*, 134115.  
 [39] T. Ablekim, S. K. Swain, W-J. Yin, K. Zaunbrecher, J. Burst, T. M. Barnes, D. Kuciauskas, S-H. Wei, K. G. Lynn, *Sci. Rep.* **2017**, *7*, 4563.  
 [40] G. Kartopu, O. Oklobia, D. Turkay, D. R. Diercks, B. P. Gorman, V. Barrioz, S. Campbell, J. D. Major, M. K. Al Turkestani, S. Yerci, T. M. Barnes, N. S. Beattie, G. Zoppi, S. Jones, S. J. C. Irvine, *Sol. Energy Mater. Sol. Cells* **2019**, *194*, 259.  
 [41] J. L. Peña, E. Hernández-Rodríguez, V. Rejón, R. Mis-Fernández, I. Riech, *IEEE 42nd Photovoltaic Specialist Conf. (PVSC)*, New Orleans, USA **2015**.  
 [42] E. Camacho-Espinosa, A. López-Sánchez, I. Rimmaudo, R. Mis-Fernández, J. L. Peña, *Sol. Energy* **2019**, *193*, 31.  
 [43] J. R. Chelikowsky, M. L. Cohen, *Phys. Rev. B* **1976**, *14*, 556.  
 [44] N. P. Brawand, M. Vörös, M. Govoni, G. Galli, *Phys. Rev. X* **2016**, *6*, 041002.  
 [45] S. Lany, A. Zunger, *Phys. Rev. B* **2008**, *78*, 235104.